ENERGETIC INTERACTIONS OF PROTONS AND PIONS

by

M. E. WILLIAMS

Presented in candidature for the degree of Master of Science of the University of Durham.

Christmas, 1962.

ABSTRACT

The thesis describes some features of the interactions of high energy protons and negative pions as observed in nuclear emulsions. A survey is given of the interactions of π^--mesons in the energy range (100 → 4,000)MeV, and in particular the optical model analysis is described. It is shown that the optical model can be made to fit the data over the whole energy range.

The interactions of 25 GeV protons are described in some detail with references to the interactions of 16 GeV π^--mesons. It is found that there is little difference between the two. Two methods of analysis of the angular distributions of produced particles, the Castagnoli analysis and the Duller-Walker plot, are described together with their application to the proton and pion induced interactions. These analyses suggest that the interaction of the proton with the nucleus is described by the cascade model. The proton makes a series of collisions with nucleons in the nucleus each of which may be inelastic and produce mesons. The struck nucleons emerge from the collisions mainly as grey particles. Those events with zero or one associated grey particle are shown to be single proton-nucleon collisions in agreement with observations of 16 GeV π^--meson interactions. The angular distribution of produced particles is found to bealmost isotropic in the centre of mass system. In the laboratory system the primary emerges from many of the interactions at small angles ($<5^\circ$).

The theory of the so called peripheral interactions, coulomb dissociation and inelastic diffraction scattering, is described and the results of a search for these interactions among the 16 GeV π^--meson events are given. A small number of such events is found and the cross-section is shown to be small.

The emulsions which were exposed to protons were also placed during the exposure in a pulsed magnetic field of 180 kilograms which was sufficient to produce a detectable curvature. The usefulness of the method is found to be limited by the degree of distortion and the accuracy of its measurement. The measurements of the 13 GeV proton interactions permitted a value of $(49 \pm 15)\%$ to be given for the inelasticity.

I

PREFACE

The material presented in this thesis describes some of the interactions of π^--mesons and protons as observed in nuclear emulsions. The study of the interactions of 16 GeV π^--mesons follows on a series of four experiments on negative pion interactions in the energy range (100 - 4,000) MeV. The searching for interactions and the measurement of angular distributions at 16 GeV has been carried out by Mr. Finney, Miss Welton and the author. The work is described more fully by P.J. Finney (Ph.D. Thesis, Durham University) who carried out most of the analysis. Again, the measurement of the interactions of 25 GeV and 13 GeV protons has been carried out by Miss Welton, Dr. Apostolakis, Dr. Major and the author, while the analysis is entirely the work of the author.

In the following pages first an outline is given of the previous work carried out on the interactions of π^--mesons, and in particular the optical model analysis is described. Then follows the analysis of the present work on high energy protons and pions with special emphasis on the proton results. Chapter 3 describes a search for a mechanism of interaction peculiar to high energies. And finally a report is given on the usefulness of pulsed magnetic fields in the determination of charged particle momenta at high energies.

CONTENTS

LIST OF FIGURES

LIST OF TABLES

CHAPTER I

A brief survey of the interactions of π^--mesons with complex nuclei between 0 and 20 GeV

Introduction

There are at least three reasons for studying the mechanism of the interactions of fundamental particles with nuclei. Firstly it is a physical phenomenon in its own right and must also be understood before other physical phenomenon can be accounted for. For example the cosmic radiation, or processes such as $K^- + p \rightarrow \Sigma^+ + \pi^-$ or $p + \bar{p} \rightarrow n\pi^{\mp}$ which, if the proton is contained within a nucleus imply further interactions by the π^- mesons escaping from the nucleus. Before this can be understood, the mechanism of the interaction of π^--mesons with nuclei must be known. Secondly it can give information on the more fundamental interactions of elementary particles with each other, and as in the case of the peripheral interactions described in Chapter 3 it can give such information which is difficult to obtain more directly. Finally it is one of the most important methods of finding out about the structure of the nucleus itself.

It has been found possible above about 100 MeV to treat the interactions of fundamental particles with the nucleus as taking place by a cascade of particle-nucleon collisions with the rest of the nucleus in each case playing a relatively small part. Thus a major problem in this study is to separate

out the effect of the secondary collisions with the nucleus from the primary collision which is assumed to take place with a single nucleon. This latter assumption is sometimes called the impulse approximation and is more true at high energies. At the same time theories have been developed which ignore the mechanism of the interaction and seek only to describe general features such as cross sections and how they change with energy. Such a theory is the optical model and will be outlined together with its application over a wide range of incident pion energies. This will be followed by a survey of the general features of the interactions of π^--mesons with nuclei as detected in emulsions. This is intended to place in perspective the results obtained at 16 GeV with π^--mesons and at 25 GeV with protons.

Optical Model Analysis

In the optical model the nuclear force field is represented by a smoothed out potential which may be complex. The incident particle is represented by a plane wave which is both scattered and absorbed by the nucleus, so distorting the plane wave. The scattering of the wave corresponds to the elastic scattering of incident particles, while the absorption of the wave corresponds to inelastic processes. The whole treatment proceeds by analogy with optical theory and the elastic scattering is essentially diffraction scattering. The degree of absorption is characterised by an absorption coefficient K which is related to the imaginary

part of the potential V_i by the relation:- (Fernbach 1949)

$$K = \frac{2V_i}{\hbar . B.c.}$$

where B.C. is the velocity of the incident particle.

The cross section for inelastic interaction, σ_a, is then given by:-

$$\sigma_a = \pi R^2 \left\{ 1 - \left[1 - (1 + 2KR) \exp(-2KR) \right] / 2K^2R^2 \right\}$$

where R is the nuclear radius.

The absorption cross section may also be computed from known free particle cross sections if a specific model for the nuclear interaction is assumed. At low energies there are two such models, for π^--meson nucleus interactions. The first model assumes that the interaction is due to the scattering of mesons by individual nucleons in the nucleus. If there is only one such collision during the interaction then the absorption coefficient is expected to be:- (Allen et al. 1959)

$$K = \left(3 / 4\pi r_0^3 \right) \sigma_{\pi^- p} \left(3 - 2\frac{Z}{A} \right)$$

where r_0 is the nucleon radius, $\sigma_{\pi^- p}$ the free cross sections for π^--meson interactions with protons, Z and A are the atomic number and atomic weight respectively.

The second model assumes that the meson is absorbed by

a proton neutron pair giving two neutrons which subsequently leave the nucleus. Then the absorption coefficient is predicted to be:-

$$K = 3 N_D . \bar{\sigma_D} / 4\pi R^3$$

where N_D is the effective number of nucleon pairs in the nucleus and $\bar{\sigma_0}$ is the absorption cross section of deuterium at the appropriate energy. Thus by a comparison between the observed and predicted values of K some information on the mechanism of the interaction is obtained. The results at various incident pion energies will now be described. (For Ref. See Table 1)

At 88 MeV, scattering by a nucleon accounted for 16% of the events. That is, in these events the meson reappeared. Charge exchange is expected to occur in a further 4% of the events. The remaining 80% is assumed to consist of π^--meson absorption. An optical model analysis gave a value for K of $\sim 4.10^{12}$ cm^{-1}. If it is assumed that only the scattering process occurs, then as described above, a value of K may be predicted and was found to be $4.5.10^{12}$ cm^{-1}. Similarly assuming only absorption predicts K to be $3.5.10^{12}$ cm^{-1}. From these values of K it is expected that scattering and absorption will occur in 60% and 40% of the stars respectively (neglecting charge exchange). The differences from the expected values can be accounted for in two ways.

The value of K, (4.10^{12} cm^{-1}) corresponds to a short

Table I

Primary Energy	Observed K $\times 10^{12}$ cm^{-1}	Calculated K	After Effect of Pauli Exclusion Principle	Comments
88 MeV (Allen 1959)	$4^{+2.5}_{-0.75}$	7.8 ± 1.6	4.4	Assumes modified gaussian distribution for nucleon momenta with cut off at 400 MeV/c.
300 MeV (Finney 1962)	1.5 ± 0.2	5.2 ± 0.3	1.7	As at 88 MeV.
750 MeV (Allen 1961)	1.5 ± 0.2	2.7	2.0 ± 0.2	Assumes Fermi distribution which inhibits production cross section completely.
4 GeV (Clarke 1957)	$2.75^{+1.25}_{-0.55}$	3	-	Pauli Effect Negligible.
16 GeV	1.5	2.4	-	Observed K very uncertain owing to possibly large degree of beam contamination.

mean free path in the nucleus and the meson may be expected to make more than one collision. At the first collision 40% will be absorbed and 60% scattered. Of the latter 40% and 60% will be absorbed and scattered at the second collision. Thus after three collisions there would be absorption in 80% of the stars. However in half of the absorptive events at least one scattering collision has occured which implies that the very large forward/backward ratio of 2.5 which is observed for black tracks in stars with a meson secondary would be in evidence for the absorptive stars. This is not so, the forward/backward ratio for the black tracks of absorptive stars being unity.

The large degree of absorption can also be explained by the reduction of the scattering cross section by the Pauli Exclusion Principle. By this principle a recoil nucleon from a scattering collision must have enough energy to lift it into an unfilled energy level for nucleons in the nucleus. The principle thus inhibits those small angle scatters which do not fulfill this condition and could account for the observed results.

At 300 MeV and 700 MeV there was a similar discrepancy between observed and predicted values for K, the values being shown in Table 1. The effect of the Pauli Exclusion Principle was calculated assuming a Fermi distribution for the nucleon momenta at both energies, while at 300 MeV better

agreement was found using a gaussion distribution with cut off at 400 $\frac{MeV}{c}$.

At 4.5 GeV the absorptive process by two nucleons is negligible. Similarly because the recoil nucleons have large momenta the Pauli Exclusion Principle has little effect. The angular distribution of scattered particles as at the lower energies is well described by the optical model, although there are some anomalously large-angle scatters. These could represent diffraction scattering off individual nucleon in the nucleus. [Steenberg 1961]. The observed value of K suggests that the pion makes on average two collisions inside the average nucleus.

The de Broglie wavelength at 16 GeV is so small that diffraction scatters are rarely observed experimentally. The optical model analysis was thus restricted to computing a value for the absorption coefficient K . Steenberg has shown that the optical model must be modified in the GeV region to take account of the granular nature of nuclear matter. This implies a certain degree of masking of one nucleon by others in the nucleus and hence a reduction in the absorption coefficient.

Conclusion

The optical model is found to describe fairly well the general features of the interactions. In order to correlate the model with the interactions of pions on free nucleons,

assumptions concerning the Pauli exclusion effect and the momentum distribution of nucleons in the nucleus have to be made. These assumptions are being examined experimentally.

Star characteristics of interactions of π^--mesons with complex nuclei

The star characteristics are the star size, the angular distribution of evaporation tracks, and of shower particles. The star size is characterized by the number of tracks falling within certain ranges of ionisation, I. The tracks are classified as shower, grey or black tracks by the following criteria:-

shower tracks, $I \leqslant 1.5\ I_{min.}$

grey tracks, $1.5\ I_{min} < I \leqslant 5\ I_{min}$

black tracks, $5\ I_{min} < I$

where I min is the minimum degree of ionisation as measured in the emulsion. The number of grey tracks N_g, and black tracks N_b, collectively form the number of heavy tracks N_h. These characteristics will be described in turn.

I. Star Sizes

These are shown in Fig. 1. Also shown for comparison are the star sizes for proton induced interactions. The diagram shows that there is little difference between the star sizes of events induced by pions and protons of a comparable energy. It is therefore unlikely that star sizes can be used legitimately to distinguish between the two types of events in cosmic radiation for example.

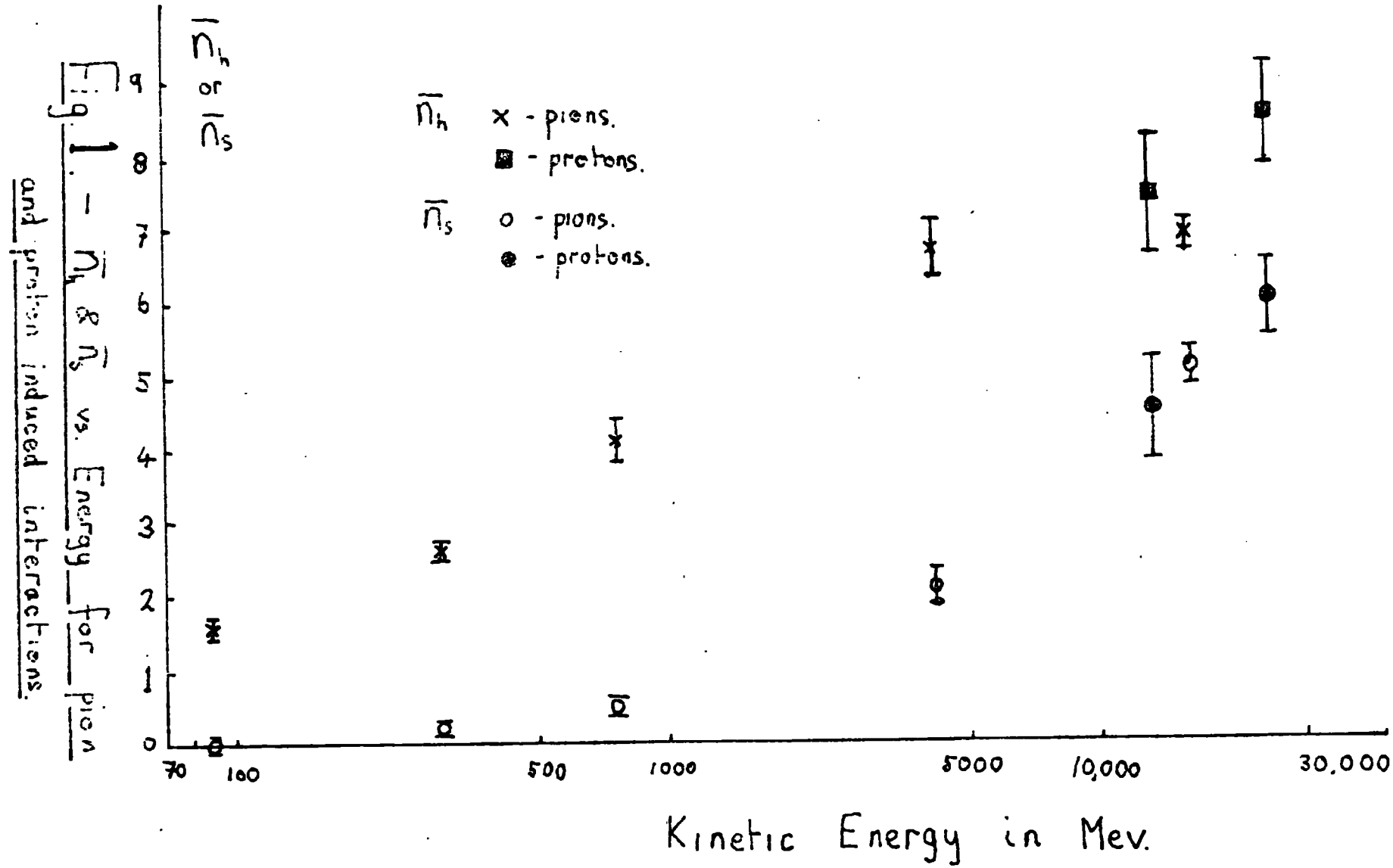

Fig. 1. - $\bar{n}_h$ & $\bar{n}_s$ vs. Energy for pion and proton induced interactions.

II. Angular distribution of evaporation tracks

The black tracks are assumed to be the tracks of ionising particles emitted by the nucleus which has been excited by the interaction. They are sometimes referred to as evaporation tracks and evaporation theory attempts to explain the energy distribution and other features of the evaporation. Since the nucleus is practically at rest in the emulsion system when it decays the distribution of tracks is expected to be isotropic with an equal forward/backward ratio. (A slight forward/backward excess might be expected if the nucleus acquires some forward momentum in the interaction).

However at 88 MeV, while the interactions in which no meson reappears have a forward/backward ratio of unity, those in which the meson continues have a ratio of 2.5. This is as yet unexplained. At higher energies the distribution is found to be almost, if not, isotropic. This is the case at 16 GeV.

III. Angular Distribution of Shower Particles

In general the shower particles will have three components Firstly the primary may continue after the interaction. This will be increasingly the case for the high incident energies when the absorption process disappears. Secondly, above the threshold for meson production such mesons will appear as shower particles or occasionally when emitted backward in

the centre of the mass system they will appear grey. Thirdly, the incident meson and the created mesons may knock nucleons out of the nucleus with sufficient energy to appear as shower particles although in general, certainly below the GeV region for the primaries they will appear grey.

At 88 MeV the scattered mesons are emitted primarily in the backward direction with a backward/forward ratio of 2.5 (This may be compared with the forward/backward ratio of evaporation tracks at the same energy also equal to 2.5). This is also explained by the Pauli effect which inhibits the small momentum transfers which contribute mainly to the forward scattering. This effect is reduced for higher energies when the shower particles become increasingly peaked in the forward direction.

When meson production sets in the angular distributions of the shower particles vary significantly from one energy to the next as different resonances and isotropic spin states come into play. Below about 600 MeV a partial wave analysis can be applied. At higher energies isobaric production appears to dominate the interaction. At 16 GeV however there are too many isobars and far too many partial waves for effective calculation and new processes may be operating. The angular distribution for shower particles at this energy will be described in some detail in the next chapter.

Chapter 2

Interactions of 25 GeV protons and 16 GeV π^--mesons with complex nuclei

Two sets of plates were exposed, one to 25 GeV protons from the proton-synchrotron at CERN, and the other to 16 GeV π^--mesons produced by the same machine. The former set of plates were placed during the exposure in a magnetic field of 180 kilogauss and the determination of momenta by means of the curvature of the tracks is described in Chapter 4. together with results obtained at 13.5 GeV. All the plates were "line scanned" and the lengths of track scanned, interaction lengths etc. are shown in Table 2. In this chapter the discussion will be mainly in terms of the interactions of the 25 GeV protons which were analysed by the author. The results however will be constantly compared with those obtained with 16 GeV π^--mesons and it will be found that, at least in their more general aspects, there is little difference in their interactions as observed in emulsions.

At these high energies a large number of mesons can be produced and the greatest interest lies in the mechanism or mechanisms of meson production. For this study some authors find a large number of events in emulsions and from

TABLE 2.

	25 GeV Protons	$\pm$6 GeV π^--mesons	13.5 GeV Protons
Length of track scanned	86.3 metres	192.5 metres	15.6 metres
Total No. of events found	234	374	46
Mean No. of heavy prongs. $\bar{n}_h$	8.5 $\pm$ 0.7	6.8 $\pm$ .4	7.4 $\pm$ 1.1
Mean No. of shower prongs. $\bar{n}_s$	6.0 $\pm$ 0.5	5.0 $\pm$ .1	4.5 $\pm$ 0.7
Interaction length in emulsion	(37 $\pm$ 2) cms	(51.5 $\pm$ 2)cms.	34 $\pm$ 6

them select those which they are reasonably sure represent collisions between the incoming particle and a single nucleon with the rest of the nucleus taking no part. However it is also of interest to find out just what effect the rest of the nucleus can have, and for this one needs to know the main features of particle-nucleon interaction. So the two studies are closely linked.

It is quite clear from the large spread in star sizes alone that at least one interaction parameter varies widely for different events. We shall examine first some of the causes for these differences.

a) Constitution of the emulsion

Nuclear emulsion contains two groups of nuclei; the light nuclei, carbon, nitrogen, and oxygen, and the heavy nuclei, sulphur, silver, bromine and iodine. These two groups differ in the number of nucleons by a factor of 7 and in nuclear size by a factor 2. Various criteria are used to distinguish between events in light and heavy nuclei. Friedländer for example suggests on the basis of results at lower energies that the events with $n_h \leqslant 4$ occur in light nuclei and events with $n_h \geqslant 7$ in heavy nuclei. Such criteria are not perfectly valid however. Somewhat more interactions are expected to occur with heavy than light nuclei. (Friedländer 1959)

b) Peripheral nuclear collisions

If the incident particle collides with a nucleon at the centre of the nucleus then both the primary and the secondaries to this initial collision will pass through a much greater distance in nuclear matter than had the initial collision taken place at the periphery of the nucleus. Thus for such events the probability of secondary collisions is greater and as we shall see, it is these secondary collisions which account for many of the observed interaction characteristics. Thus the nuclear impact parameter which is the distance between the line of flight of the primary and the centre of the target nucleus is related both to star size and angular distribution of shower particles.

c) Nucleon structure

To consider the nucleon to have a structure is perhaps extending classical concepts too far. Nevertheless in many of its interactions it appears to be characterised by a hard core of radius 0.4 fermis, surrounded by a pion cloud ranging over 1.3 fermis. In so called peripheral interactions the pion from one nucleon's cloud interacts either with the core of the other nucleon or with a pion from its pion cloud. Friedländer points out that this model can describe many features of proton interactions at accelerator energies. (Friedländer: 62). The extent to which peripheral collisions occur at these energies is not yet known.

Star Characteristics

The classification of tracks as black, grey or shower tracks was carried out visually, and it has been checked that little error is introduced in this way. The mean star sizes are given in Table 2. In Fig. 2 the mean number of heavy tracks and of grey tracks is plotted as a function of the multiplicity or number of shower tracks. The number of evaporation tracks and the number of grey tracks appear to be directly related to the multiplicity of shower tracks.

The mean multiplicity for those events with zero or one grey track was found to be 4.3 ± 0.4

This may be compared with the value found by proton-nucleon interactions to be 4.8 ± 0.3 which agrees with the value 4.95 predicted by the statistical theory of Hagedorn. (Bandinet-Robinet. 1962). The mean multiplicity for events with more than one grey track was 7.5 ± 0.4. Similarly the interactions of π^--mesons at 16 GeV which had no grey tracks had a mean multiplicity of shower tracks of 4.1 ± 0.3 The mean multiplicity for pion-proton interactions at 16 GeV is 4.1 ± 0.1 (Goldsack. 1962). Thus we may interpret those events with zero or one grey track as single collisions with one nucleon in the nucleus not followed by secondary collisions.

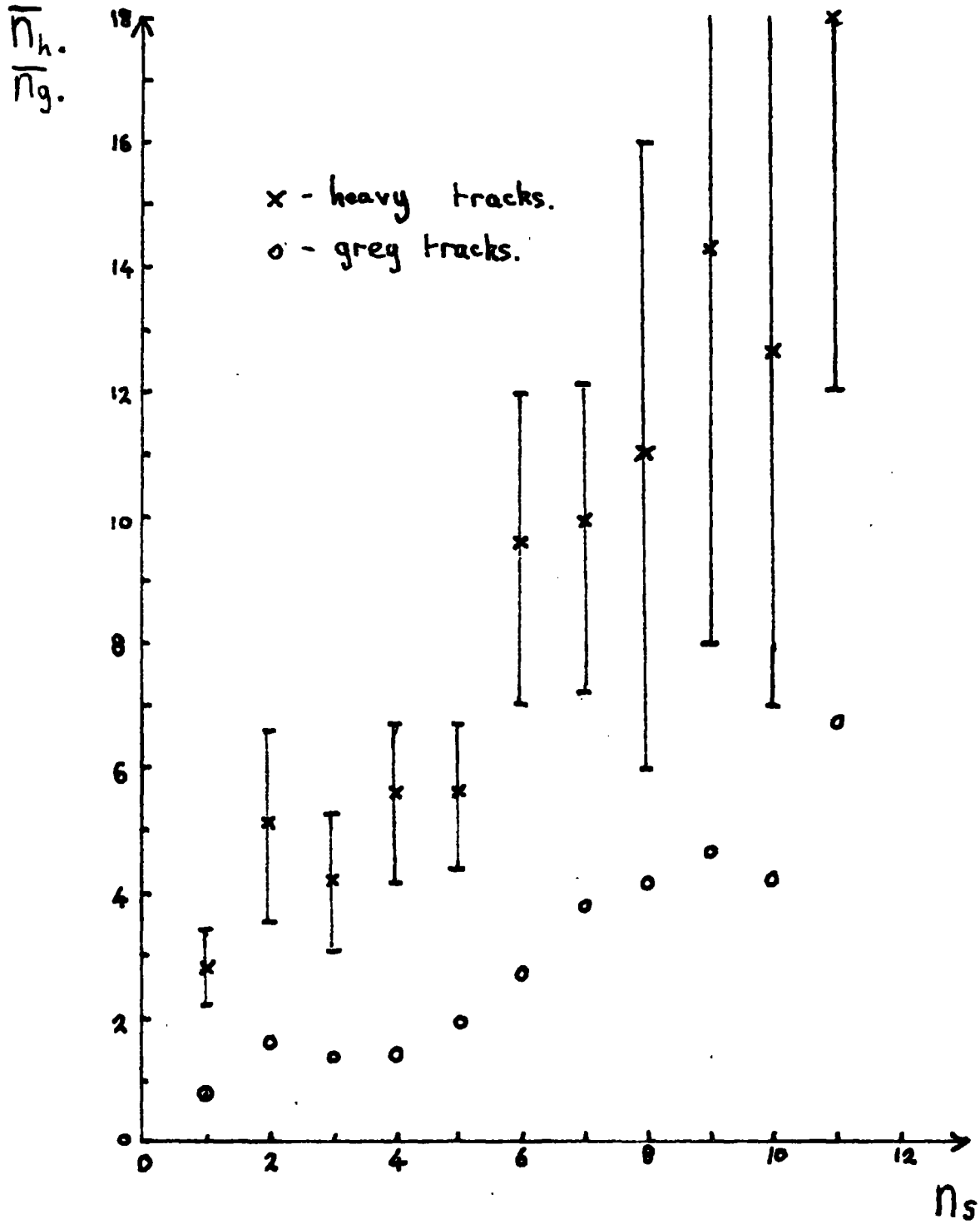

Fig. 2. - $\bar{n}_h$ & $\bar{n}_g$ vs. n_s for all events.

These star characteristics are consistent with the cascade mechanism of interaction which will now be described together with the alternative 'tube' mechanism.

Mechanism of interaction

It is shown in Chapter 3 that at high energies and subject to certain conditions, the essential region over which the interaction takes place is large and may even be as large as to involve the whole nucleus. (Feinberg & Pomeranchuk 1956).. When many mesons are produced in the first collision it is then possible that the interaction was not between the incoming nucleon (or pion) and a nucleon, but with a 'tube' of nucleons collectively. The number of nucleons in such a tube is 2.4 in light nuclei and 4.6 in heavy nuclei (Barashenkov 1959). This reference also shows that the interactions of 9 GeV protons are explicable in terms of a nuclear cascade.

In this model the mesons are produced in subsequent collisions both of the continuing primary and of the produced particles. To develop this theory quantitatively it would be necessary to perform Monte Carlo calculations over the various competing processes during the nuclear cascade. This has not been done so that it is only possible to give plausability arguments. These are derived mainly from a study of the angular distribution of shower tracks which will now be described.

Angular distribution of shower particles

To study jets, interactions at cosmic ray energies in which large numbers of shower particles are emitted in a small cone, two methods of deriving information from the angular distribution of shower particles have been developed by Castagnoli et al (1953) and by Duller and Walker (1954). They are able to derive β_c, the velocity of the centre of mass system of the interaction relative to the laboratory system, and hence the mass of the target particle if the velocity of the primary is known. The Duller-Walker method also gives information on the isotropy or degree of anisotropy in the centre of mass system. The theories are described in detail in the appendix, however the basic assumptions are as follows:-

1. The angular distribution of the produced particles in the centre of mass system is symmetric about the equatorial plane.
2. The shower particles are emitted independently of each other.
3. The velocity of the emitted particles in the centre of mass system equals the velocity of the centre of mass relative to the laboratory system. i.e. $\beta^* = \beta_c$.

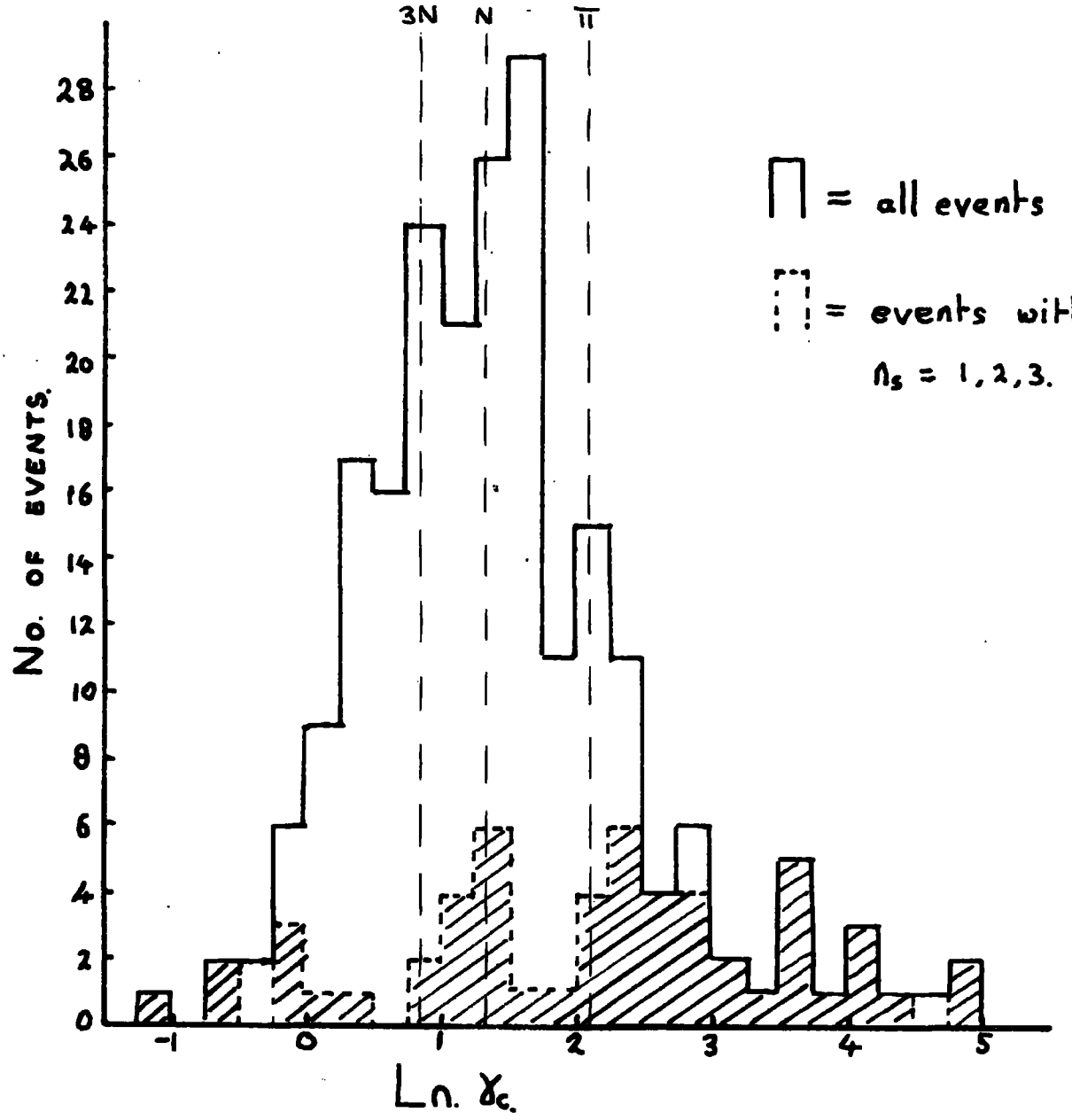

Fig.3-The distribution of ln. γ_c.

a) Castagnoli Analysis

As a consequence of these assumptions and following the notation of the appendix we have $\ln \gamma_c = \frac{1}{n_s} \sum_i^{n_s} \ln|\cot\theta_i|$.

The distribution of $\ln \gamma_c$ obtained from the 234 proton events is shown in Fig. 3. It is seen that the events of low multiplicity account for most of the tail of the distribution. These are also the events which are least likely to satisfy requirement 2. In particular the Castagnoli formula refers to produced particles and as we shall see, the primary appears to emerge from the interaction as a shower particle and this effect will show up at low multiplicities.

If the primary energy is known, then the target mass is given by the following relation (Friedländer 1959).

$$\gamma_c = \frac{(\gamma_0 + \nu)}{\sqrt{1 + \nu^2 + 2\nu\gamma_0}}$$

where γ_0 = primary energy in GeV
ν = mass of target in nucleon masses.

The expected values of γ_c are shown for various assumed target masses. It is tempting to describe the values of γ_c corresponding to a pion mass as due to peripheral collisions and those corresponding to many nucleon masses as the tube effect. However in Fig. 4. is plotted the mean values of $\ln \gamma_c$ corresponding to various multiplicities. This shows the source of the spread of $\ln \gamma_c$ values. We shall attempt to show that the deviation at low n_s is the effect of the

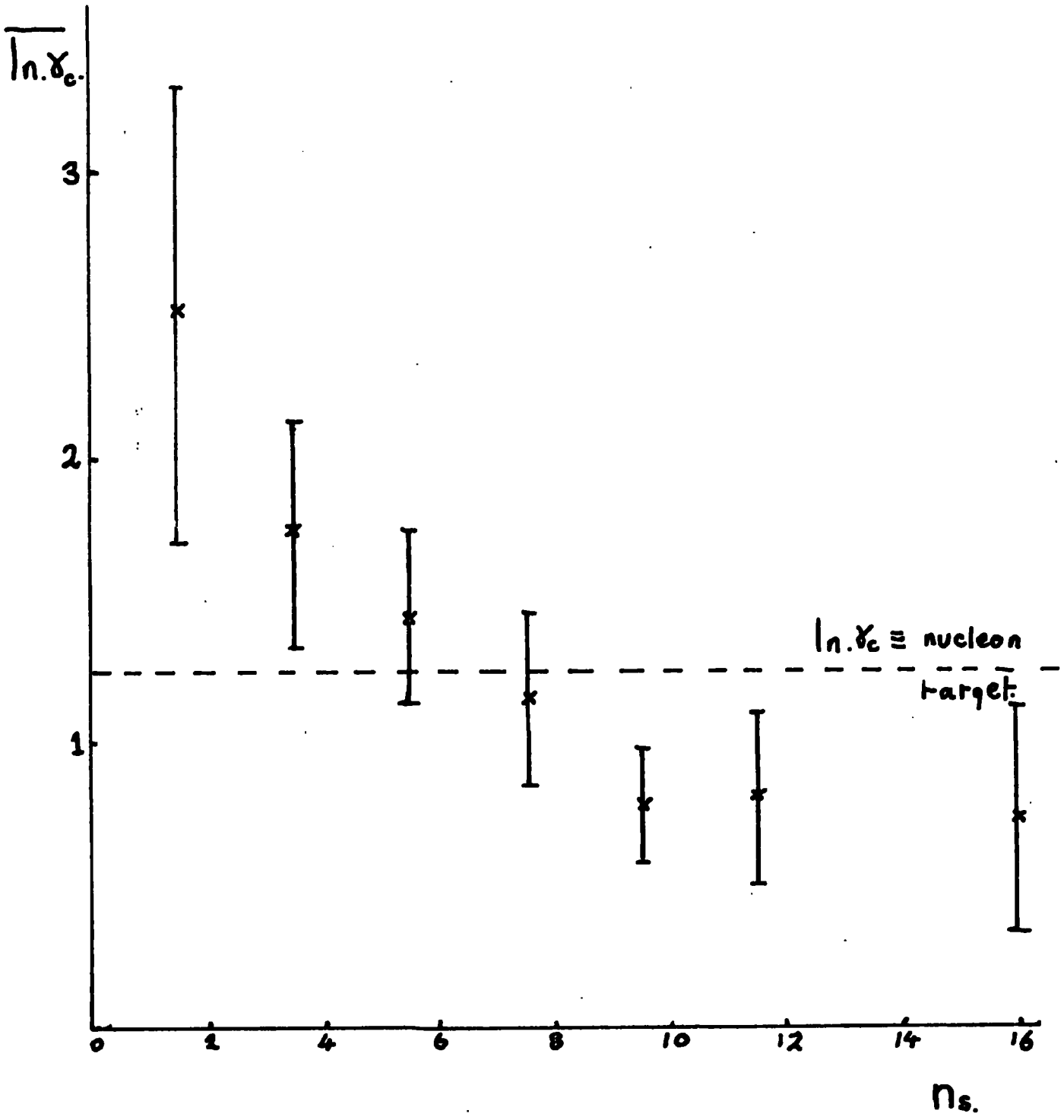

Fig. 4. - $\overline{\ln.\gamma_c}$ vs. n_s for all events. (234).

continuing primary and that for high n_s is due to secondary collisions. The errors shown are statistical and will account for the rest of the spread in $\ln \gamma_c$.

Castagnoli Analysis for $n_g = 0,1$.

It was mentioned above in connection with mean multiplicities that the events with n_g equal to zero or one could be interpreted as single proton-nucleon collisions. The values of $\overline{\ln \gamma_c}$ were thus plotted against the multiplicity for these events (Fig. 5). To test the assumption that the continuing primary affects the low n_s the values of $\ln \gamma_c$ were recomputed taking out the smallest angle in each case provided that it was less than five degrees. Some justification for this procedure is provided by the momentum measurements made on secondaries of proton interactions at 13.5 GeV described in Chapter 4. These points are also plotted in Fig. 5. (All the errors are statistical). It is seen that both for low n_s and large n_s the values of $\overline{\ln \gamma_c}$ are consistent with a one nucleon target. This analysis has also been carried out on the 16 GeV π^- interactions with the same result for n_g equal zero events.

b) Duller-Walker Plot

If the angular distribution of emitted shower particles is isotropic in the centre of mass system as well as satisfying the above three conditions then the Duller-

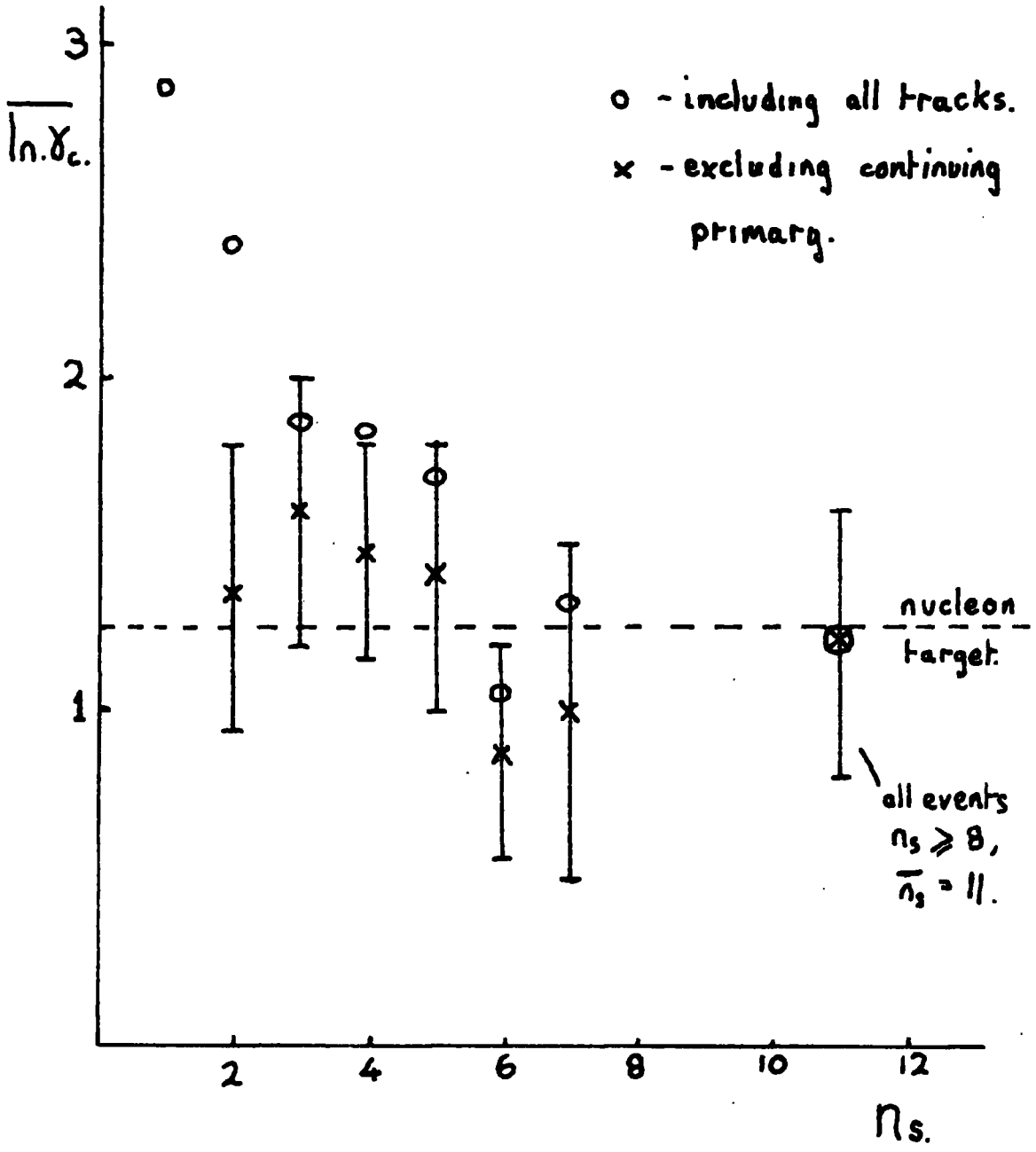

Fig. 5. - $\overline{\ln.\gamma_c}$ vs. n_s for events with $n_g = 0, 1$.

Walker plot should be a straight line of slope 2, passing through some specific point given by the expected value of γ_c. The plot is shown for all the events in Fig.6, together with the line expected for isotropy. The point for $F(<\theta) = \frac{1}{2}$ corresponds to the median angle θ_m for which $\tan\theta_m = \frac{1}{\gamma_c}$. The line drawn is that expected for a γ_c appropriate to a nucleon-nucleon collision. The experimental points indicate that for particles emitted in the forward direction in the centre of mass there are too many peaked at small angles. From the Castagnoli analysis this could be due to the primary continuing at small angles. The deviations from isotropy in the backward direction could be due to two effects. Firstly the effect of secondary collisions would be to broaden the distribution in the laboratory system. This would effectively decrease γ_c. And secondly in the primary collision the condition $\frac{\beta_c}{\beta^*} = 1$ may be violated and β^*, the velocity of particles emitted in the C.M. system might be greater than the velocity of the C.M. system in the laboratory with a consequent peaking in the backward direction. Both of these effects could cause the observed deviations at large angles. The Duller-Walker plot for the 16 GeV π^--meson interactions showed exactly the same features.

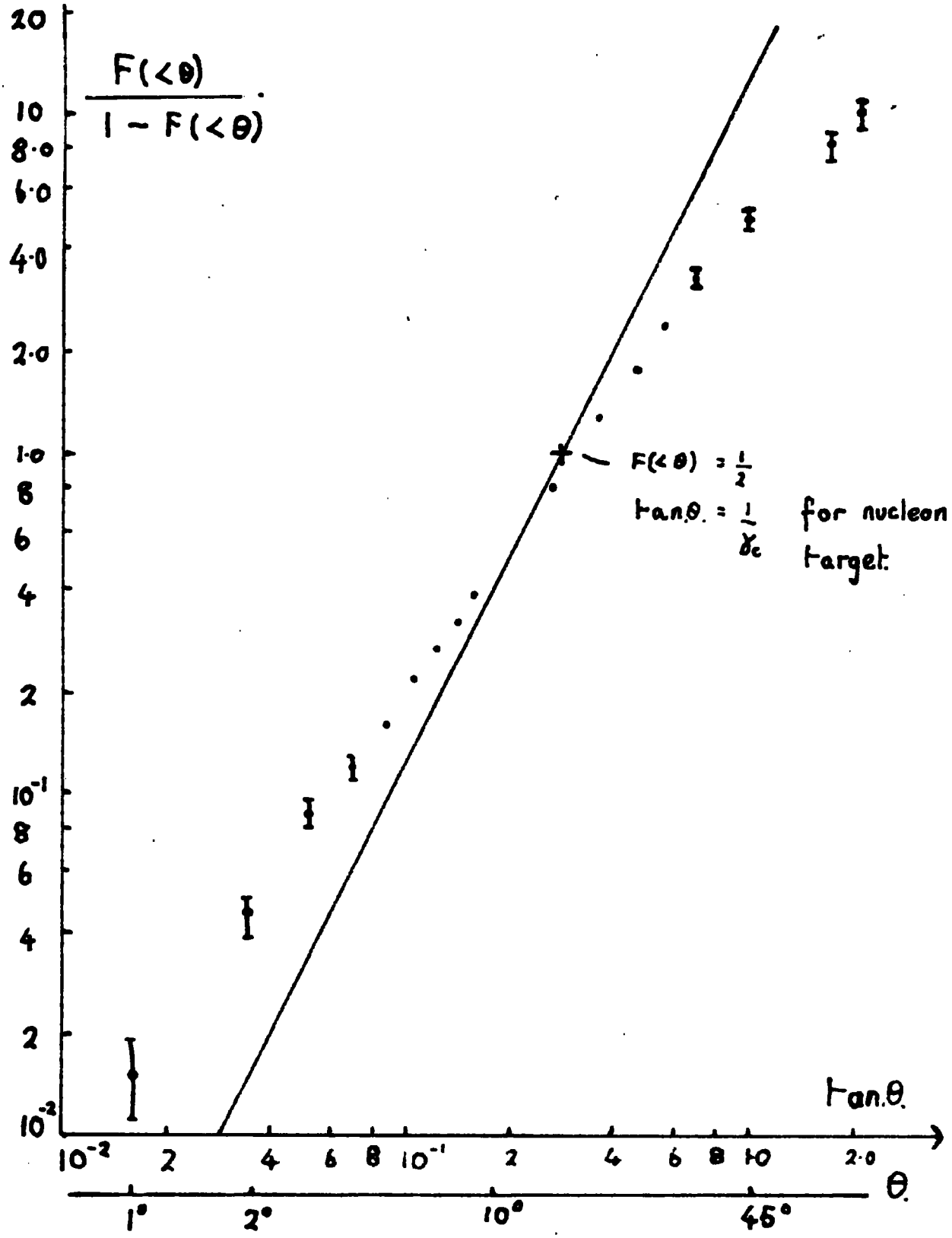

Fig. 6. – Duller - Walker (all events).

Duller-Walker for $n_g = 0,1$

Fig. 7. shows the plot for all events with $n_s > 1$ both for all observed tracks, and also excluding the particle believed to be the continuing primary. As with the Castagnoli analysis this was taken to be the particle emerging at the smallest angle provided that angle was less than 5 degrees. This was the case in 60 out of 84 events.

It is seen that the continuing primary hypothesis is supported beautifully by the plot. At large angles the deviation from isotropy is much reduced presumably by the absence of secondary collisions but some anisotropy still exists. It is noted that out of a total of about 400 tracks, 10 are emitted backwards in the laboratory system. This implies $\beta^* > \beta_c$ and accounts for the observed deviation. If these backward tracks are also excluded from the analysis the agreement is good. A similar analysis was performed on the $n_g = 0$ events for the 16 GeV π^- mesons. The behaviour is similar but there is some evidence for asymmetry in the distribution. The effects of secondary collisions and of the continuing primary are the same however.

Conclusions

1. The Castagnoli and Duller-Walker analyses may be usefully applied at Accelerator Energies.

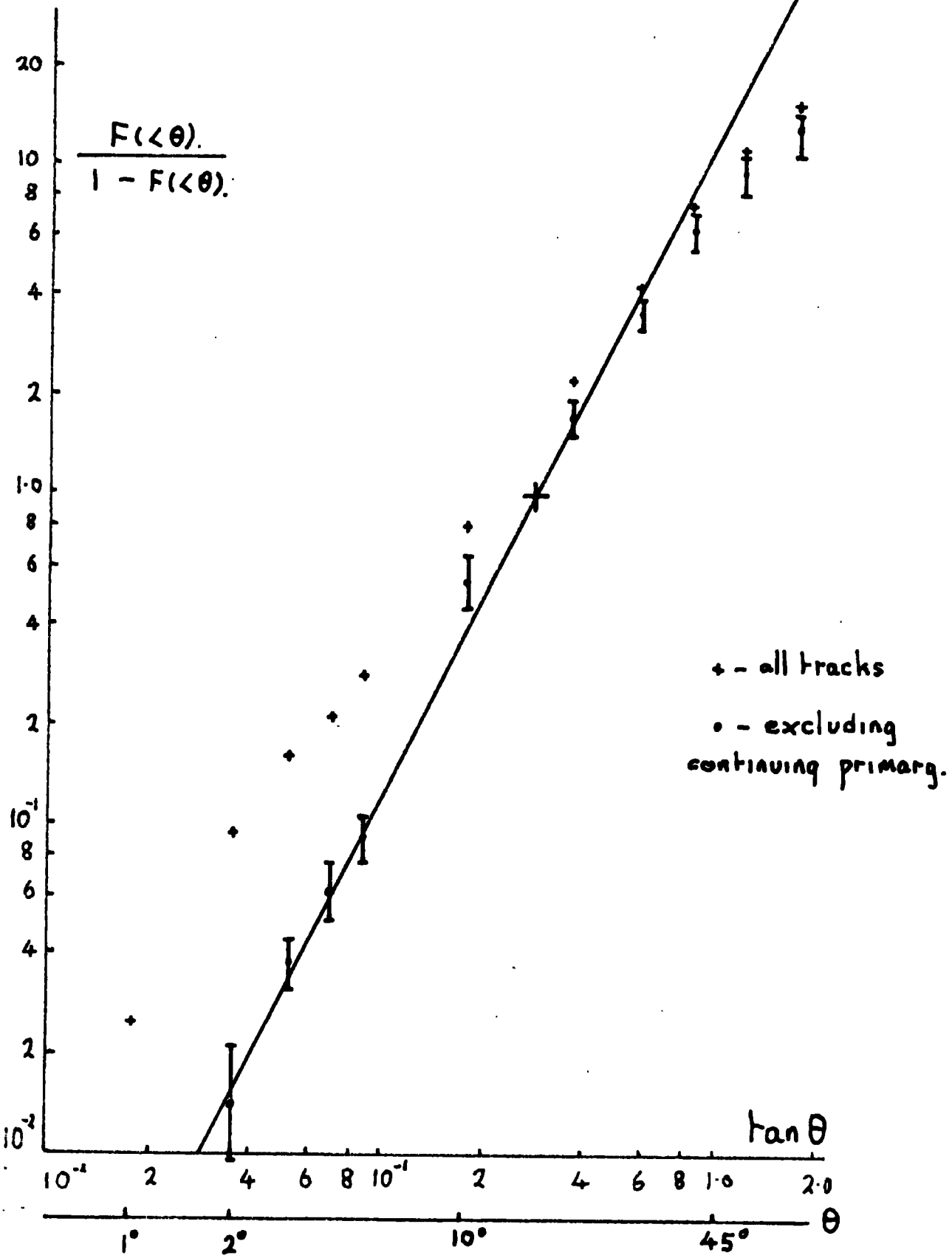

Fig. 7. – Duller-Walker for $n_g = 0, 1$

2. Events with $n_g = 0,1$ are collisions with a single nucleon in the nucleus.

3. Events with $n_g > 1$ correspond to secondary collisions taking place between the particles emerging from the primary collision and the rest of the nucleus. The grey tracks represent the struck nucleons.

4. In the initial collision the primary often continues at small angles. The produced particles are mainly isotropic in the centre of mass but there is possibly some peaking at small angles backward with $\beta^* > \beta_c$. This effect is small however with only 3% of the tracks emerging backwards in the laboratory system.

5. The effect of peripheral collisions if they occur is small.

6. For $n_g > 1$ the distribution of $\log_e \gamma_c$ peaks around an equivalent target mass of about three nucleon masses. This is interpreted as the effect of secondary collisions which broadens the angular distribution in the laboratory system. However this effect could also be interpreted in terms of the tunnel model. The single nucleon events then correspond to collisions on the periphery of the nucleus. A closer analysis of the grey particles is needed to decide definitely between the two theories. Such an analysis is being carried out by P.J. Finney on the pion interactions and seems to support the nuclear cascade model.

CHAPTER 3.

Long Range Interactions of Pions

The processes to be considered here are characterised by the interaction taking place between the incident pion and the whole nucleus. This is despite the fact that at these energies the de Broglie wavelength of the pion is sufficiently small for it to resolve individual nucleons in the nucleus and even individual pions in the pion cloud of a nucleon. The reason is as follows. As the energy of the incident pion increases, the angle of divergence of the emitted particles decreases in order to conserve angular momentum. Consequently the momentum transferred to the target decreases. By the indeterminacy relations the size of the effective interaction region increases and for sufficiently high energies may exceed the nuclear size.

Thus if a pion of energy E and rest mass m_π, interacts with a nucleus and emits a pion of energy E_π, then for small angles the longitudinal momentum transferred to the nucleus is:-

$$q_{\parallel} = \sqrt{E^2 - m_\pi^2} - \sqrt{(E - E_\pi)^2 - m_\pi^2} - \sqrt{E_\pi^2 - m_\pi^2}$$

$$\approx \frac{m_\pi^2 . E_\pi}{2E(E - E_\pi)} + \frac{m_\pi^2}{2E_\pi}$$

From the indeterminacy relation between the uncertainty in momentum and position the size of the effective interaction

region r_{eff} is given by:-

$$r_{eff} = \frac{1}{q_{\parallel}}$$

For sufficiently large values of the incident pion energy, E, the interaction region will include the whole nucleus which therefore carries away the momentum $q_{\parallel}$. Because of its large mass it carries away comparatively little energy and may remain undisrupted, and as we shall see this is the case in the energy region we are considering.

We shall first examine two postulated processes for pion production to which the above considerations apply and then examine the experimental results obtained at Durham.

A) Coulomb Dissociation

As in the previous discussion an incident pion may under certain conditions interact with the whole of a target nucleus, and if the interaction is an electromagnetic one then the pion interacts with the total nuclear coulomb field. This field may be quantised and the interaction considered to take place between the pion and a photon. That is, the process amounts to photodissociation. This is the Weizsacker-Williams approach. That this interaction results in small momentum transfer may be seen as follows.

Consider a particle of mass M and momentum P.

Its energy is $\sqrt{(P^2 + M^2)}$. If $P \gg M$ then this $= 1 + \frac{1}{2} M^2/P^2 + \ldots$

If it makes a transition to a state of mass M^* then the difference in energies is $\frac{M^{*2} - M^2}{2P}$

Thus by the indeterminacy relation between energy and time a particle of mass M may make a virtual transition to a particle of mass M^* which can exist for times of the order of $2P/\mu^{*2} - \mu^2$ For sufficiently large P the virtual state will extend over the nuclear diameter. The momentum transfer is $\frac{\mu^{*2} - \mu^2}{2P}$ so that the target particle which is the nucleus will absorb very little energy. Therefore in the process we are considering the incoming pion encounters the nucleus and absorbs a photon from the nuclear coulomb field. The momentum of this photon is sufficient to render the virtual state real. It leaves the nucleus and very rapidly decays while the nucleus balances off the momentum and remains undisrupted.

Reaction Threshold

The maximum momentum that the pion can absorb is that corresponding to the most energetic photon that can exist inside the nuclear volume. This is given by the indeterminacy relation between momentum and position.

$$\therefore q_{max} = \frac{1}{r_0 A^{\frac{1}{3}}} \simeq m_\pi A^{-\frac{1}{3}}$$

The threshold is then given by:-

$$P_{thr.} = \frac{\mu^{*2} - \mu^2}{2 q_{max}} = \frac{\mu^{*2} - \mu^2}{2 m_\pi} A^{\frac{1}{3}}$$

The reaction in which we are interested is the $\pi \longrightarrow 3\pi$ reaction in which all the particles are observable in emulsions. The threshold for this reaction is 1.3 GeV in carbon and 3.3 GeV in lead. The reaction should therefore be observable in emulsions at 16 GeV.

Reaction Cross-section (Good and Walker 1960)

If the process is considered one of photodissociation then the Weizsacker-Williams theory gives the cross-section as:-

$$\sigma = \frac{3}{2\pi} \cdot Z^2 e^2 \int_{K_{th}}^{K_{max}} \sigma_\gamma \cdot \frac{dK}{K} \cdot \ln \frac{\gamma m_\pi}{K A^{\frac{1}{3}}}$$

σ_γ = photoproduction cross-section for pion production.

K_{th} = photon threshold for this process.

K_{max} = maximum photon energy in the nuclear coulomb field.

This may be simplified by setting $\sigma_\gamma = e^2/m^2$, where m is the mass of the lightest product. i.e. the pion mass. Then the formula becomes:-

$$\sigma = \frac{3}{4\pi} \cdot \frac{Z^2 e^4}{m^2} \left[\ln \frac{2(P/m_\pi)}{\left[\left(\frac{\Pi^\pi_{min}}{m_\pi}\right)^2 - \left(\frac{\Pi^\pi}{m_\pi}\right)^2\right] A^{\frac{1}{3}}} \right]^2$$

Where, M^π = rest energy of the three pions.

$M^\pi_{min.}$ = rest masses of the three pions.

This formula gives the cross-section at 16 GeV for the

the reaction $\pi \rightarrow 3\pi$ to be 3mb in silver and 0.3mb in carbon.

A π-π resonance in the J = 1, T = 1 state has been postulated theoretically by Frazer and Fulco and has been observed in $\pi^- p$ scattering by Erwin et al. and Pickup et al. at a Q-value of about 470 MeV. By considering such a final state interaction in the π-3π reaction Ferretti has derived an expression for the $\pi \rightarrow 3\pi$ cross-section in terms of the (π-π) cross-section as follows:- (Baldessaro 1962)

$$\sigma_{\pi, 3\pi} = 10^{-8} \frac{Z^2}{A^{\frac{2}{3}}} \left(\frac{P}{m_\pi} \right)^2 \cdot \sigma_{\pi-\pi} .$$

So a knowledge of the cross-section for the Coulomb Dissociation process gives some information on the hypothetical π-π resonance.

Characteristics of the events

1) The events as seen in nuclear emulsions will consist of an ingoing minimum ionising track and three outgoing minimum ionising tracks which must be distinguished from electrons.

2) The momentum transfer in any direction and thus the longitudinal and transverse momenta must be less than

$$q_{max} = m_\pi A^{-\frac{1}{3}}$$

3) The nucleus therefore acquires energy $\sim \frac{q^2_{max}}{2MA} \leq \frac{m_\pi^2}{2MA} \sim \frac{12}{A}$ Mev and remains undisrupted. (Neutrons are of course not

observed in emulsions).

4) The energy of the secondaries must balance that of the primary.

B) Diffraction Dissociation

Elastic scattering in this energy range is essentially diffraction scattering. Because of absorptive processes the nucleus appears to the pion as an opaque or partially opaque sphere, and consequently the wavefront is distorted and the Kirchoff diffraction formulae of wave optics may be applied. On a particle picture the pion is given an impulse and consequently acquires sufficient transverse momentum to deflect it into a characteristic diffraction pattern. From the discussion on Coulomb dissociation it might be expected that this impulse could also bring about the dissociation of the pion when raised to a virtual state. Good and Walker present arguments to show that the diffraction dissociation process should be most effective with light nuclei which are semi-opaque rather than black spheres, (Good and Walker 1960), and experiments at CERN on 24 GeV protons scattered from beryllium show an inelastic peak associated with the elastic diffraction scattered peak which can be interpreted as diffraction dissociation possibly from a nucleon target. (Wetheral 1961)

Reaction Threshold

As in the case of Coulomb dissociation the threshold is determined by the requirement that the nucleus should act as a

whole. The threshold is therefore given by:-

$$P_{thr} = \frac{M^{*2} - \Pi^2}{2 m_\pi} A^{\frac{1}{3}}$$

Reaction Cross-section

The theoretical cross-section has not been estimated although rough calculations put it at less than geometrical.

Characteristics of the events

These differ from those for Coulomb dissociation only in the maximum values for the longitudinal and transverse momentum transfers.

1) The maximum value for $q_\parallel$ is limited by the requirement that the nucleus as a whole takes part in the interaction. $q_\parallel$ must therefore be less than $m_\pi / A^{\frac{1}{3}}$

2) In order that the nucleus is not disrupted the momentum transfer in any direction and therefore $q_\perp$ must be less than the inverse of the nucleon separation (Feinberg 1956).

$$\therefore \; q_\perp < m_\pi \qquad (\hbar = c = 1)$$

Thus the requirements for maximum allowed momentum transfer are less restrictive for diffraction dissociation than for coulomb dissociation. However it has not yet been found possible to separate the two processes experimentally.

Analysis of the Durham Data

The 16.3 GeV π^--meson emulsion plates as described in Chapter 2 were line scanned, and in a total of 192.5 m. of track twelve events of the type $(0 + 3)\pi$ were found. The space angles of the secondaries were measured and wherever possible their momenta. These latter measurements however were inaccurate and will not be discussed.

Since nuclear emulsions do not detect neutral particles it is necessary to distinguish between genuine trident events and those in which neutral particles are emitted. It can be shown that in a trident event, in which the momentum transferred to the nucleus is small, that for three given angles of emission the momenta of the secondary particles is uniquely determined. These momenta may be found by solving the three simultaneous equations implied by the conservation of linear momentum. The results of the computation as applied to the twelve events are shown in table 3. To check the validity of this analysis it was also applied to 38 events of the type $(N_h + 3)$ with n_h, the number of black or grey tracks associated with the event is not zero. Only one of these events gave a momentum balance. This event had one black track which suggested low nuclear excitation and so it was included among the possible trident events.

Having reduced the thirteen events to 5 possible cases of diffraction or coulomb dissociation, the requirements for

Table 3. Possible Ferretti Tridents.

Event No.	Secondary Angles in degrees. θ_1	θ_2	θ_3	Sum of Secondary Momenta. $\frac{Cqv}{c}$	$\sum_i \sin\theta_i$
1	3·28	5·45	3·59	16·33	0·21
2	1·67	1·88	7·76	16·33	0·20
3	9·80	1·47	7·33	40·45	0·32
4	25·33	12·66	8·30	156·66	0·79
5	1·14	0·50	1·63	145·04	0·06
6	5·93	2·23	32·4	80·27	0·68
7	22·66	5·00	85·0	29·15	0·49
8	2·49	1·66	2·78	$>10^6$	0·12
9	1·98	9·69	2·86	16·33	0·25
10	1·40	0·59	6·61	16·31	0·15
11	4·30	5·28	1·06	17·55 *	0·19
12	6·98	0·51	9·33	58·6	0·29
13	7·85	4·99	3·24	16·36	0·28

— (1 + 3)

* This event appeared thus, 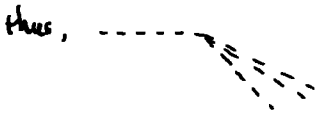 and was therefore excluded.

small momentum transfer outlined above were investigated.

In practice the momenta of the secondaries is difficult to measure accurately or at all, while the space angles can be measured with great accuracy. Use was thus made of a formula which transforms the momentum transfer requirements to angular distribution requirements. The formula is

$$\sum_i \sin\theta_i \leq \frac{q_{\perp max}}{m_\pi}$$

(Baldassaro 1960) where θ_i is the space angle of the i^{th} secondary with respect to the primary direction.

As shown above, the coulomb process is expected to predominate in elements with large atomic numbers and therefore in silver, while the diffraction process will involve mainly the lighter elements such as carbon. This leads to the following requirements being put upon the possibl dissociation events.

$$\sum_i \sin\theta_i \leq 0.44 \quad - \quad \text{diffraction process}$$

$$\leq 0.22 \quad - \quad \text{coulomb process}$$

As seen from Table 3, all five of the events which showed momentum balance (and some of those which did not) satisfy these relations.

Since the existence of these processes is hypothetical we shall consider by what alternative mechanisms the above five events could be accounted for.

a) One Pion Exchange

These processes correspond to glancing collisions with a neutron with elastic diffraction scattering off the exchanged pion.

eg.

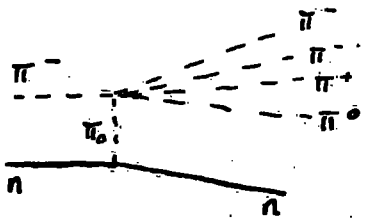

However in all events of this type at least one neutral particle is emitted. The probability of a chance momentum balance was shown above to be small.

b) Strange Particle Production

Such a process as:-

$$\pi^- + n \longrightarrow \pi^- + \Sigma^+ + K^-$$

However the excitation energy given to the nucleus by this process is calculated to be $\sim$ 150 MeV and the probability that this energy is lost solely by neutron emission is again small.

Conclusion

There appears to be no processes which can account for these five events other than coulomb dissociation and diffraction dissociation, but the experiment is unable to resolve between them.

Assuming the five events to be examples of such trident

events the upper limit of the cross section is calculated to be

$$\sigma_{\pi \to 3\pi} = 5{\cdot}4 \text{ mb. (for all elements.)}$$

This gives an upper limit to the π-π cross-section from Ferretti's formula to be:-

$$\sigma_{\pi\pi} \leq 1{,}620 \text{ m.b.}$$

CHAPTER 4.

Determination of the Momentum using Pulsed Magnetic Fields

At energies below the GeV range the momentum of ionising particles leaving tracks in nuclear emulsions is determined mainly from measurements on the degree of scattering of the track. As the energy increases the scattering becomes less detectable and measurement is only possible for track lengths of the order of centimeters. The development of pulsed magnetic fields up to 200 k-gauss uniform over several square centimeters has enabled the technique used in cloud and bubble chambers for determining the momentum from the curvature of the tracks to be used in emulsions also.

If a particle of unit charge moves with momentum p, at right angles to a uniform magnetic field H, it is deflected through a curve of radius r $\alpha \frac{p}{H}$. So by measuring r and knowing H, the value of the momentum can be determined. Some details of the field and the techniques involved in curvature and distortion measurement will be given, together with some results obtained in Durham and suggestions as to how the method could be improved.

Field Characteristics (Hoffman & Combe)

The field was produced by a Helmholtz coil energised by a bank of condensers, giving a pulse of duration of about 6 ms with a peak value of 180 kilogauss in a volume of the

order of 100 cm^3. The stacks of emulsions were roughly cylindrical with a diameter 6 cm and a thickness 1.5 cm. and were placed inside the coils with the magnetic field perpendicular to the surface of the pellicles. The protons are scattered out of the CERN proton synchrotron in bursts of duration about 1 ms. The field pulse was made to coincide with the particle burst and the synchronisation was claimed to be satisfactory. Even so, not all the particles passed through the field when it was at its maximum value as can be seen from Fig. 8. In fact the sources of error from the uncertainties in field value are as follows.

1) The voltage of the condenser bank which energises the coil varies from pulse to pulse by $\pm$ 3% and therefore the pulse height varies also.
2) The field varies by up to 4% over the volume occupied by the emulsions.
3) From Fig. 8. it is seen that 74% of the particles in a burst pass into the emulsion when the field lies within 3% of its maximum value, and for the other 26% it is within 3 and 10% lower than the maximum. This means that there will be a tail at the higher end of the measured spectra of momenta.

Curvature Measurement

Since the magnetic field was perpendicular to the emulsion pellicles the curvature of the tracks was in the

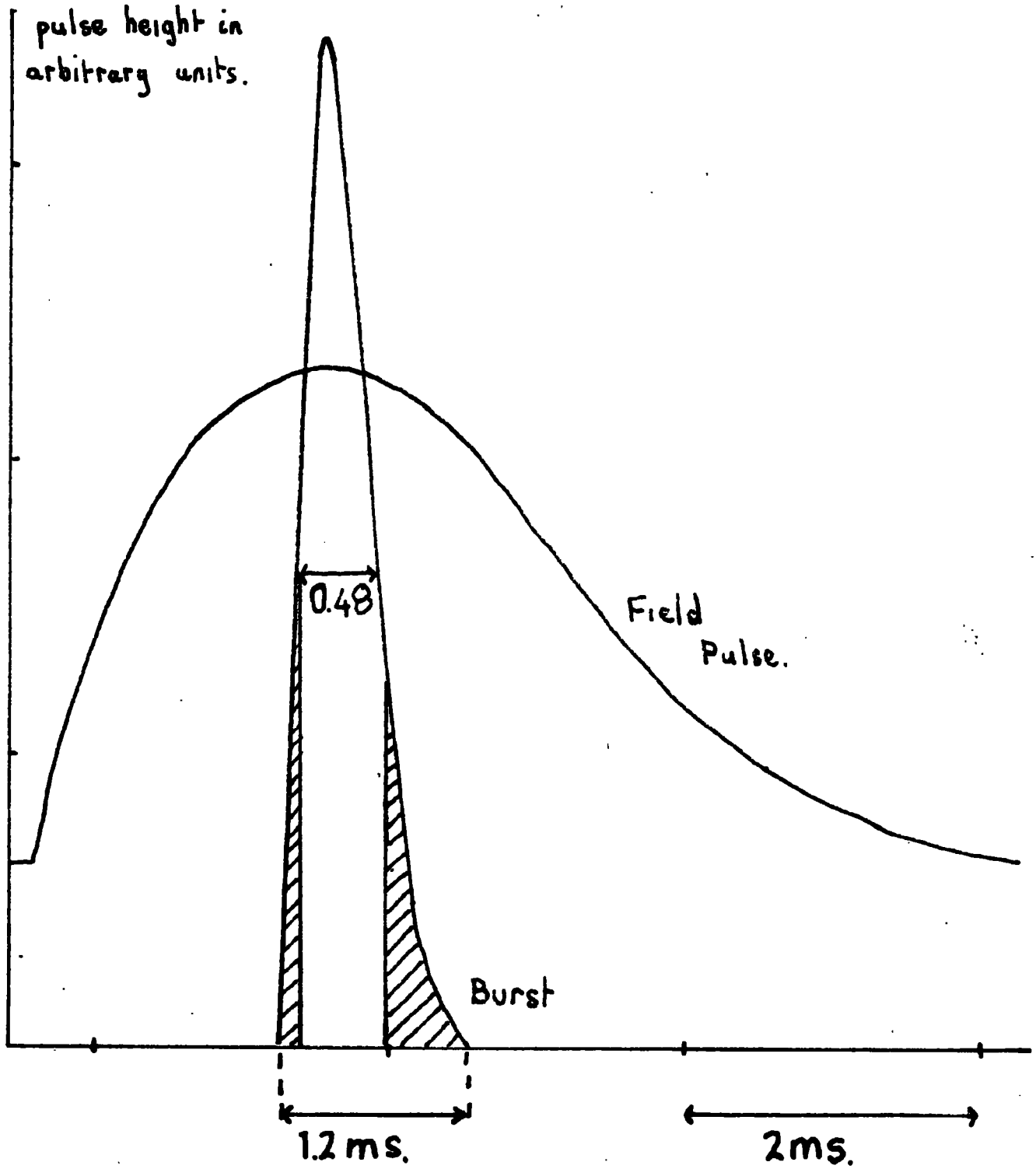

Fig. 8. Variation in time of the field pulse and particle burst.

plane of the emulsion and could thus be measured by the straight forward second difference sagitta method. The tracks were aligned so that the sagitta lay along the eye-piece scale placed in the y-direction. Three x,y,z co-ordinate readings were taken at the beginning, middle, and end of the tracks. The y-reading was taken from an eye-piece scale and second differences in the y-readings gave the sagitta D_2. The momentum of the particle is then given by:

$$pc = \frac{3 \times 10^{-4} \cdot H \cdot l^2}{D_2} \quad \text{Mev}$$

where H is the field in k gauss.

l is the cell length in microns

D_2 is the sagitta in microns.

Before this could be used to determine the momentum a correction for the distortion had to be made.

Distortion Correction

At some time during the processing of the plates a relative displacement in the planes of the emulsion takes place. This means that a straight track which is not flat in the plane of the emulsion will appear curved after processing and a curved track will have its curvature altered. To measure this displacement additional exposures were made to the beam in which relativistic tracks were made vertically

through the pellicles. Two methods of distortion correction were used and will be described.

Method A

This method was used with the 13.5 GeV plates in which the distortion was fairly small ($K_2 \sim 15u$) and could in fact be neglected for tracks of pronounced curvature. The density of vertical tracks was for the most part sufficiently high so that with a field of view two or three could be seen. Then the displacement of the track under measurement was determined from the displacement at the same height of nearby vertical tracks. This displacement was then subtracted from the measured y-coordinate of the track at that point, and upon taking second differences the effect of distortion is eliminated.

Method B

The 24.5 GeV plates differed from the 13.5 GeV in certain respects. Firstly the density of vertical tracks was not consistently high and the tracks were not accurately vertical. Secondly the distortion was at least twice as large, and thirdly the emulsions appeared to have been buckled during the exposure. Therefore upon sticking down and processing, tracks which had been flat in the emulsion now appeared to rise towards the middle of the plate and fall at the edges.

With method A, inconsistent results were obtained and

so the distortion was measured more directly. The distortion vector at each point was determined and the displacement computed from the formula (Apostolakis and Major 195)

$$\Delta = K_2 \left[-2\left(\frac{d}{T}\right) + \left(\frac{d}{T}\right)^2 \right]$$

where Δ = displacement

K_2 = distortion vector

T = emulsion thickness

d = height of track

Errors in distortion measurement

The variation of distortion is largest at the bottom surface of the emulsion. This makes it difficult to pick out the exact spot where the vertical distortion tracks enter the emulsion and constitutes the greatest source of error in distortion measurement. For this reason whenever possible 4 distortion measurements were made and the average taken.

Multiple Scattering Errors

The multiple scattering which at lower energies can be used to determine particle momenta becomes here a noise upon which is superimposed the magnetic curvature. The signal to noise ratio, or in other words the ratio of the angle θ_m produced by magnetic curvature, to θ_c, produced by multiple scatter in track length t is given by:-

$$\frac{\theta_m}{\theta_c} \simeq 6 \times 10^{-5} . \text{ H. B. } \sqrt{t}$$

where H = field in gauss

B = scattering constant.

Therefore as long a track length, t, as possible is used. For t = 0.4 cm the error on the curvature measurement is ~ 12%, for t = 1.2 cm the error is about 6%.

It is possible by a somewhat complicated procedure to combine both the multiple scattering estimate and the magnetic estimate of the momentum to achieve greater accuracy, particularly in sign determination. However the gain in accuracy does not appear to compensate for the increase in labour.

Results obtained.

One plate exposed to 13.5 GeV protons was "line scanned" and 42 events found. The primaries of all these stars were measured to ensure that they were in the field. The spectrum of primary energies obtained is shown in fig. 9. . The tracks were fairly flat and the distortion was small so that the spread about 13.5 GeV is assumed to be due to the field characteristics described earlier. [The beam was claimed to have a momentum spread of less than 3%]. The measured value of the primary was then used to normalise subsequent momentum measurements on each event.

The spatial angles of the secondaries of each event were

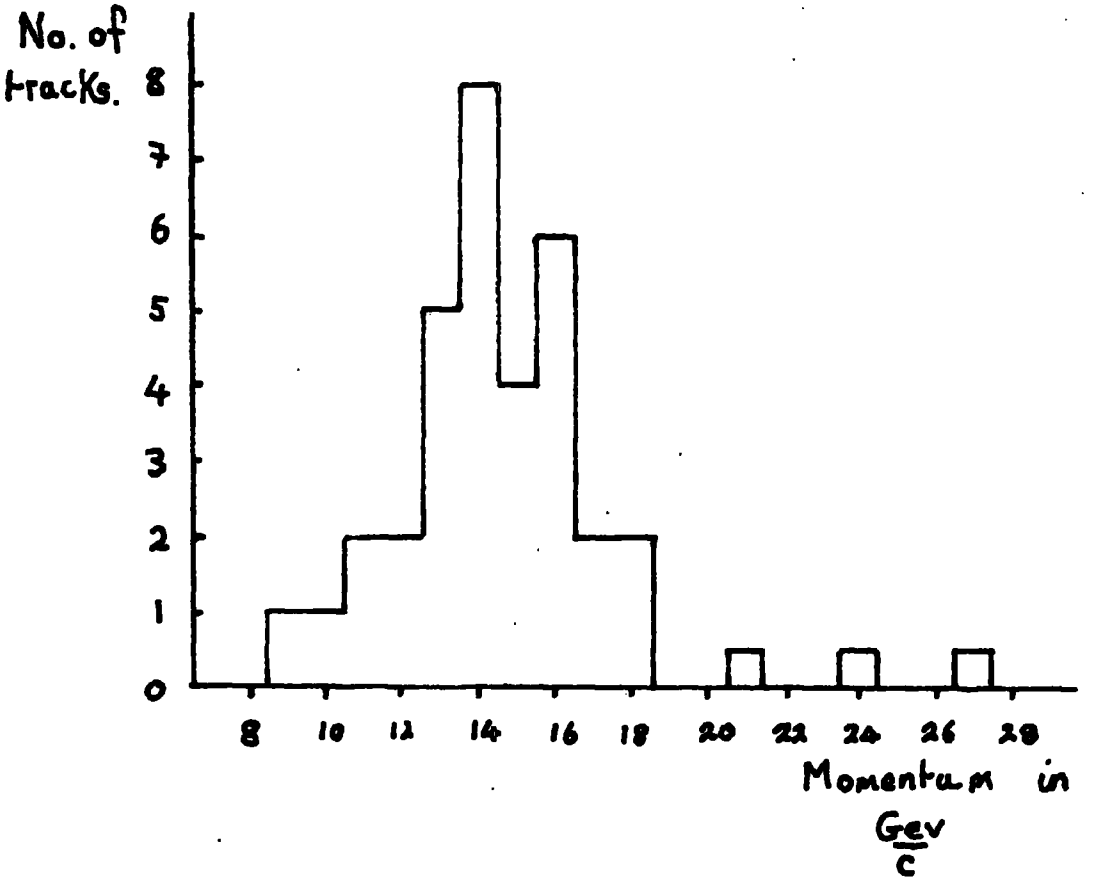

Fig. 9. - Distribution of primary momenta for 13·5 Gev/c proton induced interactions.

measured by recording the coordinates of two points on each track. The stage was then rotated to bring each secondary in turn along the horizontal axis of the eye piece scale and if the track was long enough its curvature was measured. No rigid criterion was laid down for this but in general, if a curvature could be detected in following the secondary then it was measured. There was a certain degree of compensation in that short tracks were those with large space angles which tended to have lower momenta and hence large curvatures. The sign of the secondary is given by the sign of the second difference.

Transverse momentum for 13.5 GeV.

The transverse momentum distribution of secondary particles is of particular interest since it remains invariant under the Lorentz transformation from the centre of mass system, and because it can be used to distinguish between various theories of meson production at high energies.

Altogether 80 secondaries were measured from 29 events which had measurable tracks. Of these 56 were positive and 24 negative, giving a $\pm$ ratio of 2.5. If it is assumed that the incoming proton continues in each case then the $\pm$ ratio for produced particles is about unity. Of the secondaries with space angles less than five degrees, twelve are positive and two negative suggesting that it is the incident proton continuing.

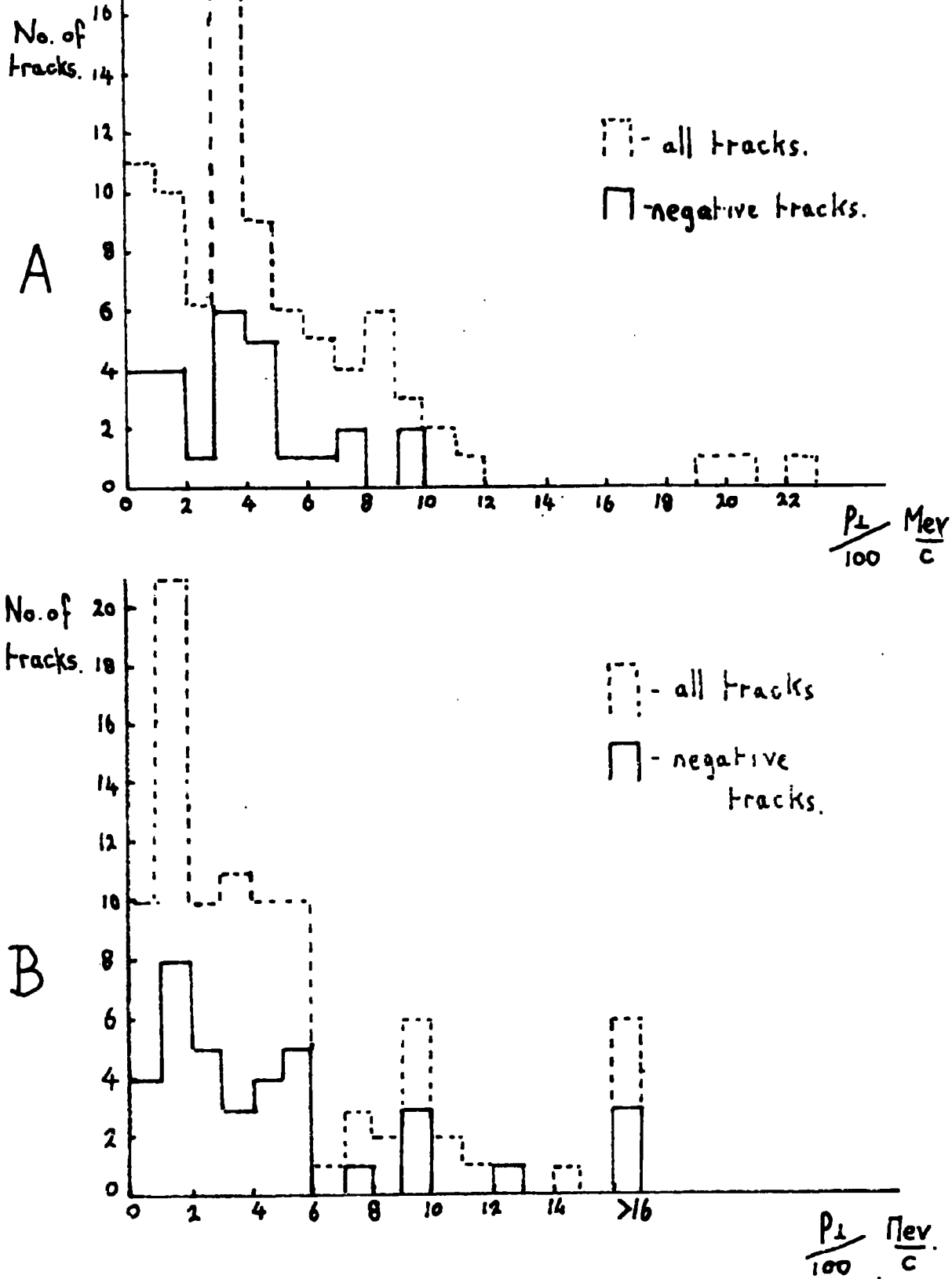

Fig. 10- Transverse Momentum distribution.

A - 13·5 Gev Proton Primary Energy.

B - 24·5 Gev. Proton Primary Energy.

Event	N_g	N_s	Most energetic secondary (GeV/c)	Spatial angle in degrees	Energy in other measured tracks	Comments	Inelasticity
1	0	3	+5.9	1.5	5		56%
2	0	3	+2.7	13.4	-	unmeasured track at 8.6°	
12	0	3	+7.9	6.1	1.7		42%
15	0	2	+9.3	17.5	0		31%
22	0	4	+5.4	8.2	4.4		60%
23	0	3	+0.6	36	0.5	possible charge exchange	(95%)
30	0	6	+0.7	83	0.7	unmeasured track at 3.5°	
41	0	2	+2.3	8.4	2.1		83%
4	1	6	+4.8	10.4	4.4		64%
5	1	1	+13.3	3.6	0	scatter?	(0%)
14	1	1	+11.3	0.7	0		16%
26	1	2	+11.9	2.3	0		12%
31	1	5	-3.7	5.5	0	unmeasured track at 3.3°	-
37	1	3	+12.4	2.3	3		?
38	1	9	-2.5	10.9	2.3	possible charge exchange	-
39	1	5	+7.5	3.0	3.5		44%
17	2	4	+3.2	6.2	0.8		76%
40	2	3	+8.4	3.4	0		38%
10	3	4	+5.9	2.1	6.2		56%
36	4	3	+9.7	3.3	0		28%
3	4	6	+4.6	4.6	0.3		64%
13	5	8	+3.3	16.9	10.1		75%
19	5	6	+2.5	26.4	0	unmeasured track at 18.7°	-
8	6	8	-2.7	36	5.4	possible charge exchange	-
11	7	10	+6.3	9.3	3.9		53%
16	6	7	+10.4±3	10.8	4.8		23%
20	7	8	+4.5	11.8	2.7		67%
29	8	8	+2.2	18	0	unmeasured track at 3.5°	-
							mean = 49%

The transverse momentum distribution is shown in Fig. 10 The mean values are:-

$\bar{p}_\perp$ for positive particles = 450 MeV $\pm$ 90 (excluding particles of momentum >1.5 GeV)

$\bar{p}_\perp$ for negative particles = 340 MeV $\pm$ 70

It will be noted that the particles with large transverse momentum are predominantly positive and could be the continuing primary. These values are in agreement with those obtained by other authors at similar energies, but the errors are so large that this is hardly ssignificant.

Inelasticity at 13.5 GeV

The inelasticity of an interaction is defined as the proportion of available energy going into particle production. As with the transverse momentum distribution it is a parameter which enables different mechanisms of particle production to be distinguished experimentally. Currently of interest is the supposition that peripheral interactions of low inelasticity dominate the interaction at these energies. The primary should thus continue with a large proportion of its original energy, at small angles. By measuring the energy of the most energetic positive secondary a lower limit for the inelasticity is directly obtained.

The results are shown in Table 4 . It is seen that in seventeen events the most energetic secondary measured has

the smallest space angle and is very probably the continuing primary. For these events the inelasticity is 49% ± 15%.

The uncertainty is large, but there is certainly little evidence for a very low inelasticity.

Results at 25 GeV

These plates presented much greater difficulty of measurement than the 13.5 GeV plates, for the following reasons.

1. Only about half the events proved to have taken place while the field was on.
2. All the energies are higher and the curvature consequently more difficult to measure.
3. The distortion was greater in these plates.
4. Many of the events suffered from severe clouding and image fading due to faulty processing.

For these reasons the momentum of the primary either could not be measured or was determined with a very large error. All secondary momenta are therefore given unnormalised.

Transverse Momenta

The measured distribution is shown in Fig. 10. There appears to be little difference between either the general shape of the distribution or the mean values of the transverse momenta at 25 $\frac{\text{GeV}}{c}$ and 13.5 $\frac{\text{GeV}}{c}$. However the near equality of the mean transverse momentum for positive and negative tracks, and the absence of any high momentum positive tail suggests

that the proton primary emerges from the interaction with a lower proportion of its energy than at 13.5 GeV.

These considerations suggest that the inelasticity is lower at 25 than at 13.5 $\frac{\text{GeV}}{c}$. This is supported by the observation that in few of the events was a high energy positive secondary detected. This is partly accounted for by the difficulty in detecting the curvature of such high momenta tracks.

$\bar{P}_\perp$ for positive particles = 396 ± 80 Mev.

$\bar{P}_\perp$ for negative particles = 406 ± 80 Mev.

Comments on the Usefulness of Magnetic Fields with Emulsions

The usefulness of the method is limited by three factors.

a) The time required to carry out the measurements

b) The limit on the accuracy

c) Bias introduced by unmeasurable tracks.

The time taken to measure the momentum of a track was found to depend mainly upon the facility of distortion measurement. This measurement was hampered by the low density of vertical tracks which necessitated searching the area around the event for them, and also by the fact that the vertical tracks were not exactly vertical thereby introducing error and necessitating the somewhat more involved method B.

The accuracy was found to be limited by the accuracy with which the distortion correction could be determined. Again, more vertical tracks would help and of course as careful a development as possible to keep the general level of distortion as low and as uniform as possible. Clearly higher fields and thicker emulsions would increase the accuracy and also decrease the bias caused by tracks whose tracklength is too small to be measured.

Ultimately, as in most emulsion experiments, the usefulness of the method reduces to a question of time and statistics. However with a little improvement the pulsed magnetic field could be a very useful tool in the study of nuclear interactions

in emulsions at any rate in the region of 13 GeV.

APPENDIX

A. Castagnoli Analysis (Castagnoli et al. 1953)

Notation

$c\beta_c$ = velocity of the centre of gravity with respect to the laboratory.

$c\beta^*$ = velocity of emitted particles in the centre of mass system.

θ = angle of emission of a particle measured in the laboratory.

θ^* = angle of emission of a particle in the centre of mass system.

$$\gamma_c = \frac{1}{\sqrt{1-\beta_c^2}}.$$

Now θ is related to θ^* through the transformation:-

$$\gamma_c = \frac{1}{|tg\,\theta|} \cdot \frac{(1-\cos^2\theta^*)^{\frac{1}{2}}}{\left|\cos\theta^* + \frac{\beta_c}{\beta^*}\right|}.$$

Taking logarithms on both sides gives

$$\ln \gamma_c = -\ln|tg\,\theta| + u\left(\cos\theta^*, \frac{\beta_c}{\beta^*}\right) \quad \text{where, } u = \ln \frac{(1-\cos^2\theta^*)^{\frac{1}{2}}}{\left|\cos\theta^* + \frac{\beta_c}{\beta^*}\right|}$$

Summing over all emitted particles, N_S gives:-

$$\ln \gamma_c = -\frac{1}{n_s}\sum_{1}^{n_s} \ln|tg\,\theta_i| + \frac{1}{n_s}\sum_{1}^{n_s} u\left(\cos\theta^*, \frac{\beta_c}{\beta^*}\right)$$

Assume, a) that the angular distribution of all the N_S emitted

particles is symmetric with respect to the equatorial plane in the centre of mass system.

b) that there is no correlation between their angles or their energies of emission.

If it is further assumed that $\frac{\beta_c}{\beta^*} = 1$ then it is shown that $\ln \gamma_c$ should be distributed about a mean value $\frac{1}{n_s} \sum_{i}^{n_s} \ln |\cot \theta_i|$ with a variance $\frac{\sigma}{\sqrt{n_s}}$, where $\sigma \sim \frac{\pi}{\sqrt{12}}$.

Thus the expectation value of $\ln \gamma_c$, is the mean value of $\ln |\cot \theta|$.

B. Duller-Walker Analysis (Duller and Walker 1954)

Let F be the proportion of tracks contained within the angle θ in the laboratory or θ^* in the centre of mass system. Then for an isotropic distribution in the centre of mass we have

$$F = \frac{1}{2}(1 - \cos\theta^*)$$

$$\therefore \frac{F}{1-F} = \left(\frac{\sin\theta^*}{\frac{\beta_c}{\beta^*} + \cos\theta^*} \right)$$

If it is again assumed that $\frac{\beta_c}{\beta^*} = 1$ then the transformation for θ to θ^* gives $\frac{F}{1-F} = (\gamma_c \cdot \tan\theta)^2$

$$\therefore \log_{10} \frac{F}{1-F} = 2\left(\log_{10} \tan\theta - \log_{10} \frac{1}{\gamma_c}\right)$$

thus a plot of $\log\left(\frac{F}{1-F}\right)$ against log tan θ should be a straight line of slope 2 provided the assumptions are justified.

Note that when $F = \frac{1}{2}$

$$\log_{10} \frac{F}{1-F} = 0$$

$$\therefore \tan \theta_{\frac{1}{2}} = \frac{1}{\gamma_c}$$

Acknowledgments

The author wishes to acknowledge the assistance given by all the members of the Durham University emulsion group - Miss Welton, Mr. Finney, Dr. Apostolakis, and the scanners Miss McCavanagh and Mrs. Errington. In particular he wishes to thank his supervisor Dr. Major for assistance and guidance.

The work was carried out under the terms of a D.S.I.R. Advanced Course Studentship.

REFERENCES

Allen et al., 1959, Phil. Mag., 4, 858.

Apostolakis and Major, 1957, Brit. J. App. Phys., 8, 9.

Baldessaro, 1960, Proc. Aix en Provence, Conference on elementary particles.

Baldessaro, 1961, Nuovo Cimento, 21, 459.

Barashenkov, 1959, Nuc. Physics, 14, 522.

Baudinet-Robinet, 1962, Nuc. Phys., 32, 452.

Castagnoli et al., 1953, Nuovo Cimento, X, 1539.

Clarke and Major, 1957, Phil. Mag., 2, 37.

Duller and Walker, 1959, Phys. Rev., 93, 215.

Erwin et al., 1961, Phys. Rev. Letters, 7, 39.

Feinberg and Pomeranchuk, 1956, Nuovo Cimento Supplement, 3, 652.

Fernback, 1949, Phys. Rev., 75, 1352.

Finney et al., 1962, Phil. Mag., 7, 237.

Frazer and Fulco, 1960, Phys. Rev., 117, 1609.

Friedländer, 1959, Nuovo Cimento, 14, 796.

Friedländer, 1962, Phys. Rev., 127, 247.

Goldsack, 1962, Nuovo Cimento, 23, 941.

Good and Walker, 1960, Phys. Rev., 120, 1855.

Hoffman and Combe, 1962, Nuc. Instruments, 15, 51.

Pickup et al., 1961, Phys. Rev. Letters, 7, 192.

Steenberg, 1962, Nuc. Phys., 32, 381.

Wetheral, 1961, Rev. Mod. Phys., 1.

Allen et al, 1961, Phil Mag 6, 833.